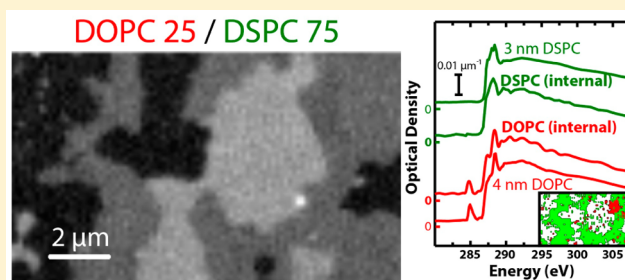


# X-ray Absorption Spectroscopy and Spectromicroscopy of Supported Lipid Bilayers

Jonathan D. West,<sup>1b</sup> Yujie Zhu, Sokunthearath Saem,<sup>1b</sup> Jose Moran-Mirabal,<sup>\*1b</sup> and Adam P. Hitchcock<sup>\*1b</sup>

Department of Chemistry and Chemical Biology, McMaster University, Hamilton, Ontario L8S 4M1, Canada

**ABSTRACT:** The C 1s, O 1s, and N 1s X-ray absorption spectra of three lipid species, 1,2-dioleoyl-*sn*-glycero-3-phosphocholine (DOPC), 1,2-distearoyl-*sn*-glycero-3-phosphocholine (DSPC), and 1,2-dioleoyl-3-trimethylammonium-propane (chloride salt) (DOTAP), have been recorded using transmission detection in a scanning transmission X-ray microscope. The spectra are presented on an absolute intensity scale (i.e., optical density per nm) to allow their use as reference standards for spectromicroscopic analysis of supported lipid bilayers. Examples of C 1s based spectromicroscopic mapping of saturated and unsaturated domains in dry lipid bilayers of DOPC and DSPC at several compositions are presented. The results are compared with fluorescence microscopy of the same area. Challenges for extending this work to studies of wet lipid bilayers interacting with antimicrobial peptides are discussed.



## 1. INTRODUCTION

Lipids are a diverse class of molecules that form the basis of the cell plasma membrane and perform various essential functions in all living species.<sup>1</sup> Lipids can self-assemble into an amphipathic bilayer with a thickness between 4 and 8 nm, which serves as the cell and organelle boundary. Such lipid membranes serve many important biological functions including the ability to control the passage of molecules based on their size and charge.<sup>2</sup> This fundamental property of bilayers has made them a focal point for contemporary research in the fields of cell biology, drug delivery,<sup>1</sup> and disease diagnosis.<sup>3</sup> Experimental methods to study lipid bilayer samples, both pristine and after interactions with other species, are required to advance these fields. In this case, the ultimate aim of this work is the study of mechanisms of interactions of cationic antimicrobial peptides with anionic model membranes.<sup>4,5</sup>

Many analytical techniques, including dual polarization interferometry, atomic force microscopy, electron microscopy, neutron scattering, X-ray microscopy, and X-ray scattering, have been used to characterize lipid bilayers.<sup>6</sup> Optical microscopy techniques, such as confocal fluorescence microscopy, have also been used to map phase segregation in both giant unilamellar vesicles<sup>7</sup> and supported lipid bilayers (SLBs).<sup>8,9</sup> In this work, we have developed reliable methods to deposit phase-segregated lipid bilayers from mixtures of saturated and unsaturated lipids onto silicon nitride windows and have monitored the spatial distribution of the deposited species through fluorescence microscopy. These bilayers were then measured using scanning transmission X-ray microscopy (STXM)<sup>10</sup> with the goal to develop the STXM method to the point where it can identify and quantitatively map heterogeneous lipid bilayer structures.

STXM was first used to study lipids in natural environmental biofilms,<sup>11</sup> and there have been many subsequent STXM studies in which signals from lipids are mapped in various types of biological and environmental systems. However, to date none of these studies have achieved single bilayer sensitivity. Prior soft X-ray microscopy studies of lipid bilayer systems include: STXM of lipid multilayers with incorporated proteins;<sup>12</sup> X-ray photoemission electron microscopy (X-PEEM) investigations of protein and peptide interactions with candidate phase-segregated polymer blends;<sup>13</sup> STXM and X-PEEM studies of interactions of antimicrobial peptides with lipid membranes;<sup>14–16</sup> and STXM analysis of lipid-decorated nanostructures.<sup>17</sup> Carrascosa et al.<sup>18</sup> used soft X-ray full field microtomography at 510 eV to visualize lipid membranes enclosing *Vaccinia* virus particles. These studies showed that despite weak signals from the monolayer and even submonolayer amounts involved it was possible to achieve sufficient signal quality to identify chemical species, measure the amounts present, and perform chemical mapping at sub 100 nm lateral spatial resolution. Encouraged by these results, we set out to explore the ability of STXM to identify and quantitatively map heterogeneous lipid bilayer structures, with the goal of later extending the method to include studies of peptide interactions with the phase-segregated bilayers in controlled aqueous environments.

STXM uses tunable focused soft X-rays to measure spatially resolved near-edge X-ray absorption fine structure (NEXAFS) spectra. If sufficient sensitivity can be achieved, then STXM would be able to map a heterogeneous lipid bilayer sample in its native hydrated state, without the use of labels. In addition

Received: March 20, 2017

Revised: April 9, 2017

Published: April 11, 2017

to high spatial resolution and absence of labels, STXM is advantageous relative to analytical electron microscopy because radiation damage per unit spectral information is approximately 2 orders of magnitude lower in STXM than in core level electron energy loss spectroscopy (EELS).<sup>19,20</sup> The major challenge of applying STXM to lipid bilayers is the extremely weak optical density of a  $\sim 5$  nm thick layer. While total electron yield (TEY) detection could in principle be used to enhance surface sensitivity, this would restrict the method to dry samples, whereas the systems of real interest are fully hydrated, to which TEY cannot be applied. Thus, the emphasis in this work is to use transmission geometry which allows for later extension to lipid bilayers with an aqueous overlayer of suitable thickness and composition.

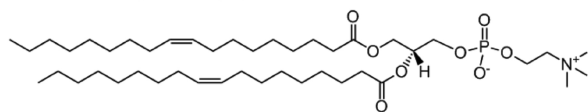
Nonspatially resolved NEXAFS spectroscopy studies of lipids have been reported previously. Panajotović et al.<sup>21</sup> measured N 1s and O 1s total electron yield spectra of single layers of 1,2-dipalmitoyl-*sn*-glycero-3-phosphocholine (DPPC) on Au prepared using Langmuir–Blodgett deposition. Franz-Daniel et al.<sup>22</sup> measured C 1s NEXAFS of a self-assembled monolayer of a prelinked unsaturated lipid bilayer structure: 3-((14-((4-0-((5-methyl-1-phenyl-3-5-(phytanyl)oxy)-6,9,12,15,18,21,24,27,30,33,37-undecaoxa-2,3-dithiaheptacantan-51-yl)oxy)-[1,1 0-biphenyl]-4-yl)oxy)tetradecyl)oxy)-2-(phytanyl)oxy glycerol (FMTS) on Au, both as formed and after interaction with CCGW(VELPPP)<sub>3</sub>, a proline-rich amphipathic peptide. Tsukada et al.<sup>23</sup> reported the N 1s spectrum of phosphatidylcholine (PC) liposomes tethered to Au nanoparticles in aqueous solution. Our results are compared to the spectra reported in those papers.

This paper presents the C 1s, O 1s, and N 1s X-ray absorption spectra of three lipid compounds: 1,2-dioleoyl-*sn*-glycero-3-phosphocholine (DOPC), 1,2-distearoyl-*sn*-glycero-3-phosphocholine (DSPC), and 1,2-dioleoyl-3-trimethylammonium-propane (chloride salt) (DOTAP). The structures of these molecules are indicated in Scheme 1. The spectra were measured from multilayer, solvent-cast deposits on silicon

**Scheme 1. Structure of the Lipid Species Studied in This Work**

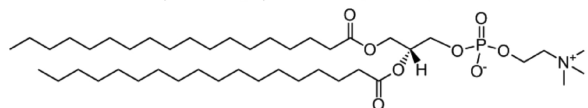
**DOPC** C<sub>44</sub>H<sub>84</sub>NO<sub>8</sub>P

1,2-dioleoyl-*sn*-glycero-3-phosphocholine



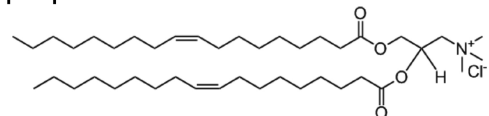
**DSPC** C<sub>44</sub>H<sub>88</sub>NO<sub>8</sub>P

1,2-distearoyl-*sn*-glycero-3-phosphocholine



**DOTAP** C<sub>42</sub>H<sub>80</sub>NO<sub>4</sub>Cl

1,2-dioleoyl-3-trimethylammonium-propane chloride



nitride windows using STXM and converted to absolute intensity scale (OD/nm). The reference spectra were then used to quantitatively map the constituent lipids contained within (i) multilayer phase-segregated lipid structures deposited from chloroform solutions and (ii) phase-segregated, supported lipid bilayer (SLB) films prepared from aqueous solutions and examined under dry conditions. STXM mapping of the multilayer is compared to fluorescence optical microscopy of the same area. The combination of the reference spectroscopy and demonstration mapping of dry SLBs sets the stage for further development of STXM as a tool to investigate fully hydrated SLBs in static or flow systems.

## 2. EXPERIMENTAL SECTION

**2.1. Sample Preparation.** All lipids, purchased from Avanti Polar Lipids (Alabaster, AL) in powder form, were used as received, dissolved in HPLC-grade chloroform to a stock concentration of 25 mg/mL, and stored in glass vials sealed with Teflon-coated caps at  $-14$  °C until needed. Lipid samples for spectroscopy were prepared in piranha-cleaned 2 mL glass vials using the stock lipid solutions and drop-cast onto piranha-cleaned silicon nitride windows (SiN<sub>x</sub>, Norcada Inc., Edmonton, AB, Canada) which were rendered hydrophilic by oxygen plasma treatment.<sup>24</sup> DOPC and DSPC mixtures were prepared by accurately measuring the appropriate volumes from the chloroform stock solutions to obtain the desired molar ratios and thoroughly mixing them into 1 mL of chloroform. In samples used for fluorescence imaging, Lissamine Rhodamine B 1,2-dihexadecanoyl-*sn*-glycero-3-phosphoethanolamine triethylammonium salt (DHPE-LR) (Life Technologies, Carlsbad, California) was added to the mixture at a 1 part per thousand (ppt) level as a fluorescent probe.

For lipid samples cast directly from solvent, a 50:50 molar ratio of DOPC/DSPC and 1 ppt DHPE-LR was prepared in a 1:1 (v/v) mixture of trifluoroethanol and chloroform to make a 0.01 mg/mL (total lipid) solution. Then, 15  $\mu$ L of the solution was drop-cast onto a preheated SiN<sub>x</sub> window maintained at 70 °C and incubated for 5 min to allow rapid drying, followed by drying in a vacuum oven at room temperature for 4 h to ensure complete removal of the solvent. The drop-cast thin lipid films were then annealed at 60 °C for 24 h under ambient conditions, before the temperature was decreased slowly at a rate of 5 °C/hour, allowing the lipids to rearrange into phase-segregated lipid bilayers.

For samples cast from aqueous solutions onto SiN<sub>x</sub> windows, a chloroform solution containing the desired lipid mixture was vacuum-dried overnight to remove the solvent and form a lipid cake. The lipid cake was then resuspended in 1 $\times$  phosphate buffer saline (PBS, consisting of 137 mM NaCl, 2.7 mM KCl, 10 mM Na<sub>2</sub>HPO<sub>4</sub>, and 1.8 mM KH<sub>2</sub>PO<sub>4</sub>; VWR, Mississauga ON, Canada) to yield a 1 mM lipid solution which was then vigorously vortex-mixed to generate large multilamellar vesicles (LMVs). The LMV solution was filtered through a 0.45  $\mu$ m pore poly(ether sulfone) filtering membrane (Whatman, GE Life Sciences, Mississauga, ON, Canada) to reduce the vesicle size. The lipid solution was then warmed to 70 °C to ensure both DSPC and DOPC were perfectly mixed in the liquid disordered phase and to facilitate extrusion. The warm solution was extruded 11 times through a 100 nm pore polycarbonate membrane filter (Whatman, GE Life Sciences, Mississauga, ON, Canada) using a mini-extruder (Avanti Polar Lipids, Alabaster, AL) to generate a 1 mM solution of small unilamellar vesicles (SUVs). A diluted 0.2 mM SUV solution was then used

to form lipid bilayers on various substrates including mica, SiN<sub>x</sub> wafers, untreated SiN<sub>x</sub> windows, and pretreated hydrophilic SiN<sub>x</sub> windows (Norcada, Edmonton, AB, Canada). A 15  $\mu$ L volume of the 0.2 mM SUV solution was pipetted onto a clean SiN<sub>x</sub> window sitting in a glass Petri dish and left to incubate for 1 h at 70 °C in a lab-built humidified chamber, consisting of a sealed plastic container with a water reservoir, which was placed inside an Ecotherm IN-30 benchtop incubator (Torrey Pines Scientific, Carlsbad, CA) to promote vesicle fusion and the formation of a supported lipid bilayer (SLB). The 70 °C temperature ensured that both lipids were in the liquid disordered phase since the gel to liquid transition temperature for DSPC is 55 °C while that for DOPC is -17 °C.<sup>25</sup> The substrate was then removed from the incubator, and 5 mL of warm (70 °C) 1 $\times$  PBS was added to the Petri dish and removed without allowing it to dry. This rinsing process was repeated five times with 3 mL aliquots of warm 1 $\times$  PBS to remove excess vesicles that did not adhere to the substrate. The PBS covered substrate was then placed back into the incubator at 70 °C and cooled to 50 °C at a rate of 0.1 °C/min to allow phase segregation and then cooled to room temperature at a rate of 0.5 °C/min.

In order to prepare the bilayer STXM samples, the SLBs were dried by first reducing the buffer salt concentration through successive washes with 1 $\times$ , 0.75 $\times$ , 0.5 $\times$ , 0.3 $\times$ , and 0.1 $\times$  PBS, rinsing thoroughly each time. The buffer was then removed and replaced with Milli-Q water. The bilayer films were then subjected to fluorescence imaging; the Milli-Q water was removed by wicking off with a wipe and the sample left to dry overnight. The dry window was then mounted on a STXM support plate and imaged in transmission and fluorescence mode to identify areas of interest for STXM analysis. While this section has presented the sample preparation procedures for the specific samples for which results are presented, other sample preparation approaches and conditions were explored. Further details of the sample preparation and its optimization are given in the M.Sc. thesis of the lead author.<sup>24</sup> We also draw the reader's attention to related work on optimization of SLB formation by Ratto et al.,<sup>26</sup> Kraft et al.,<sup>27</sup> and Mantil et al.<sup>28</sup> With regard to optimization of dry SLB structures, please consult the work by Seu et al.<sup>29</sup> on surface treatments and that by Ricker et al.<sup>30</sup> on methods to preserve phase separation through the drying process.

**2.2. Fluorescence Microscopy.** Fluorescence microscopy (FM) was used to monitor sample preparation, optimize bilayer formation,<sup>24</sup> identify suitable areas for STXM, and provide a direct comparison of FM and STXM images of the phase-segregated domains. In these experiments, DHPE-LR was used as the fluorescent probe since it is known to partition preferentially into the liquid disordered phase<sup>8</sup> and would primarily label the DOPC-rich phase at room temperature. Fluorescence recovery after photobleaching (FRAP) tests were used to confirm the formation of mobile bilayers on the substrates. The samples, which were prepared on mica, SiN<sub>x</sub> wafers, untreated SiN<sub>x</sub> windows, and pretreated hydrophilic SiN<sub>x</sub> windows, were imaged using a Nikon Eclipse LV100N POL epifluorescence microscope (Nikon Instruments, Mississauga, ON, Canada) equipped with excitation and emission filters for Rhodamine dye, and a 60 $\times$ /0.5NA physiological objective. Images were acquired with a Retiga 2000R cooled CCD camera (QImaging, Surrey, BC, Canada) and recorded with the NIS-Elements AR software (Nikon, Tokyo, Japan). The quality of the phase segregation was highest for wet

samples (1 $\times$  PBS overlayer) on mica or hydrophilized SiN<sub>x</sub>, worse for wet nontreated SiN<sub>x</sub> windows, and always degraded from the drying process. Despite the unfavorable nature of dried SLB films, we could find areas on many samples with phase-segregated bilayer regions suitable for STXM and FM analysis. In many cases, impurities and collapsed SLB were observed, often in the form of 50–200 nm lipid deposits.

**2.3. STXM.** STXM measurements were performed using the polymer STXM<sup>31</sup> on beamline 5.3.2.2<sup>32</sup> at the Advanced Light Source (ALS, Berkeley, CA) or the ambient STXM on beamline 10ID1<sup>33</sup> at the Canadian Light Source (CLS, Saskatoon, SK, Canada). As-measured transmission images were converted to optical density (OD) images using the Beer–Lambert Law,  $OD = \log(I_0/I)$ , where  $I_0$  is the incident photon flux measured through a blank area of the SiN<sub>x</sub> window and  $I$  is the photon flux transmitted through an area where the sample is present. Since there was only partial coverage of the sample by the SLBs, lipid bilayer areas were identified using the difference in OD images measured at 288.5 eV (peak C 1s signal from lipids) and at 280 eV (below the C 1s onset). A full C 1s image sequence (also called a stack)<sup>34</sup> from 280 to 340 eV was then measured on areas typically 10  $\mu$ m  $\times$  10  $\mu$ m using 100 or 200 nm steps and with the STXM beam defocused to match the step size. Radiation damage to lipids is a concern and the reason why we chose to use defocused beam sizes, which reduced the dose by 10–40 times relative to the use of a fully focused  $\sim$ 30 nm spot. The photon energy step size was 0.10 eV from 284 to 290 and 0.25 eV or larger outside this region.

Axis2000<sup>35</sup> was used for stack alignment, conversion to OD, and singular value decomposition mapping<sup>36</sup> using the lipid reference spectra measured in this work. The spectra of the pure lipids, measured with good statistics from a multilayer deposit, were converted to optical density per nanometer (OD1) intensity scale, by scaling the intensity such that the signal below the onset of edge structure and the signal far above the NEXAFS transitions (typically 30 eV above the edge onset) matched the spectrum of the same elemental composition computed from tabulated elemental cross sections,<sup>37</sup> the molecular formula (Scheme 1), 1 nm thickness, and a density of 1.0 g/cm<sup>3</sup>. Although a density of 1.480 g/cm<sup>3</sup> is listed by the manufacturer,<sup>25</sup> this corresponds to the density of the chloroform solvent, not the lipid itself. In our case, we use STXM to measure the thickness of dried lipid material in its stable, solid-state form. The density of solid lipids<sup>24</sup> was estimated to be 1.0 g/cm<sup>3</sup>, by comparison to the densities of stearic acid (an 18-carbon carboxylic acid) which is 0.941 g/cm<sup>3</sup> at 20 °C<sup>38</sup> and of 18:1 PC which is 0.975 g/cm<sup>3</sup> at 20 °C.<sup>39</sup>

### 3. RESULTS AND DISCUSSION

**3.1. Reference Spectra of Lipids.** Figure 1 presents the C 1s spectra of DOPC, DSPC, and DOTAP. The spectra are presented on an absolute intensity scale (OD/nm or OD1 scale), which is important for their use as reference spectra for absolute thickness determinations. Energies and proposed assignments for the spectral features are listed in Table 1. The strongest signal in the C 1s spectrum of each species is at 288.5 eV, which corresponds to the C 1s(C=O)  $\rightarrow$   $\pi^*_{C=O}$  transition from the carboxylate in the lipid headgroup. C 1s(C=O)  $\rightarrow$   $\pi^*_{C=O}$  transitions are well-known to be quite sensitive to the local environment of the carbon atom.<sup>40</sup> Values for carboxylate groups range from 288.2 to 288.7 eV, with values at lower energies occurring in systems where the carboxylate is conjugated with a ring system. The characteristic

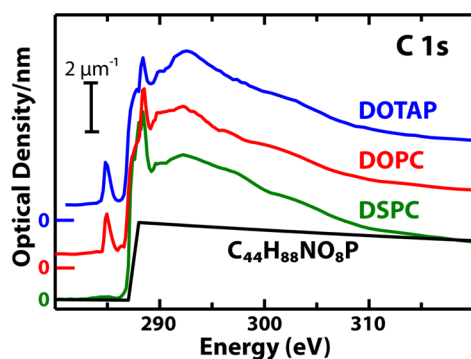


**Figure 1.** C 1s spectra of DOPC, DSPC, and DOTAP. The spectra have been scaled to match the predicted elemental response of 1 nm at  $d = 1.0 \text{ g/cm}^{-3}$ . The elemental response for DSPC (thin black line) is plotted as an example of the procedure used to derive the optical density per nm (OD1) intensity scale. See text for further details.

energy for  $\pi^*$  transitions in carboxylate species has been noted by other researchers using C 1s spectromicroscopy.<sup>41–44</sup> The C 1s spectra of two of the three lipid species, DOPC and DOTAP, exhibit a transition at 285.1 eV, which is the C 1s( $\text{C}=\text{C}$ )  $\rightarrow \pi^*_{\text{C}=\text{C}}$  transition at the unsaturated carbon-carbon double bond in the aliphatic tail of these species. The absence of a 285.1 eV peak with simultaneous exhibition of the characteristic 288.5 eV lipid carboxylate peak is the way to differentiate saturated lipids like DSPC from unsaturated lipids like DOPC and DOTAP in mixed lipid bilayers. Compared to prior NEXAFS studies, our C 1s spectrum of DSPC is better resolved but otherwise similar to the C 1s spectrum of DMPC

(also a saturated lipid) reported by Nováková et al.<sup>12</sup> Relative to our C 1s spectrum of DOPC, the C 1s spectrum of DOPC reported by the same group shows much more structure in the 300–317 eV region. Given that this region of the spectra of all three species are so similar in our work, we believe the structure in the 300–317 eV region reported by Nováková et al.<sup>12</sup> is an artifact.

Figure 2 presents the N 1s spectra of DOPC, DSPC, and DOTAP on an OD1 intensity scale. Energies and proposed

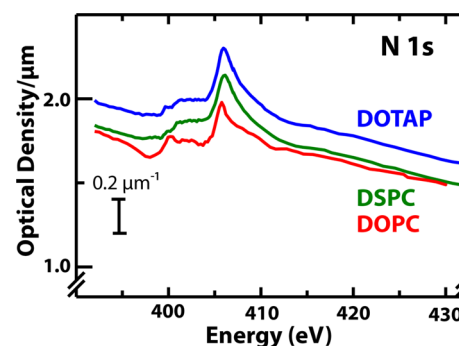


**Figure 2.** N 1s spectra of DOPC, DSPC, and DOTAP presented on an absolute OD1 intensity scale (OD/nm).

assignments for the spectral features are listed in Table 1. The amount of nitrogen in the lipids is small, but the presence of this signal, with a very similar, characteristic spectral shape in each of the lipid species and with a shape that is consistent with the presence of a quaternary ammonium group in each

**Table 1.** Energies and Tentative Assignments for Spectral Features in the X-ray Absorption of DOPC, DSPC, and DOTAP

		C 1s			proposed assignments		
#		energy (eV)			C=C	CH <sub>2</sub>	CO <sub>2</sub>
		DSPC	DOPC	DOTAP			
1			285.0	285.0	$\pi^*_{\text{C}=\text{C}}$		
2	287.4 (sh)		287.5 (sh)	287.6 (sh)		$\sigma^*_{\text{C-H}}$	
3	288.47 <sup>a</sup>		288.48 <sup>b</sup>	288.52 <sup>c</sup>			$\pi^*_{\text{C=O}}$
4	289.9		289.9	289.9		$\sigma^*_{\text{C-C}}$	
5	292.2		292.3	292.6		$\sigma^*_{\text{C-C}}$	
6	304		302	302			$\sigma^*_{\text{C=O}}$
		N 1s			proposed assignments		
#		energy (eV)			NMe <sub>3</sub>	other	
		DSPC	DOPC	DOTAP			
1		399.3	399.9	399.8		N=C (?)	
2	402.1 (sh)		402.4 (sh)	402.1 (sh)			
3	405.9 <sup>a</sup>		406.1 <sup>b</sup>	406.1 <sup>c</sup>	$\sigma^*_{\text{N-C}}$		
4	409 (sh)		410 (sh)	410 (sh)	$\sigma^*_{\text{N-C}}$		
		O 1s			proposed assignments		
#		energy (eV)			C=O	C(=O)-O	P=O
		DSPC	DOPC	DOTAP			
1		532.0 <sup>a</sup>	532.2 <sup>b</sup>	532.2 <sup>c</sup>	$\pi^*_{\text{C=O}}$		
2	534.9 (sh)		535.2 (sh)	535.3 (sh)		$\pi^*_{\text{C=O}}$	
3	538.5 (br)		539.5 (br)	539.9 (br)		$\sigma^*_{\text{C-O}}$	$\sigma^*_{\text{P-O}}$
4	546 (sh)		547 (sh)	547 (sh)	$\sigma^*_{\text{C=O}}$		

<sup>a</sup>DSPC energy calibration: C 1s  $-6.47(5)$  eV from C 1s  $\rightarrow 3p$  transition of CO<sub>2</sub> [ref 54], N 1s  $-1.2(1)$  eV from N 1s  $\rightarrow 3p$  transition of N<sub>2</sub> [ref 55], O 1s  $-6.9(1)$  eV from O 1s  $\rightarrow 3s$  transition of CO<sub>2</sub> [ref 56]. <sup>b</sup>DOPC energy calibration: C 1s  $-6.48(5)$  eV from C 1s  $\rightarrow 3p$  transition of CO<sub>2</sub> [ref 54], N 1s  $-1.0(1)$  eV from N 1s  $\rightarrow 3p$  transition of N<sub>2</sub> [ref 55], O 1s  $-6.7(1)$  eV from O 1s  $\rightarrow 3s$  transition of CO<sub>2</sub> [ref 56]. <sup>c</sup>DOTAP energy calibration: C 1s  $-6.44(5)$  eV from C 1s  $\rightarrow 3p$  transition of CO<sub>2</sub> [ref 54], N 1s  $-1.0(1)$  eV from N 1s  $\rightarrow 3p$  transition of N<sub>2</sub> [ref 55], O 1s  $-6.7(1)$  eV from O 1s  $\rightarrow 3s$  transition of CO<sub>2</sub> [ref 56].

molecule,<sup>45,46</sup> can be used to confirm molecular identity. The peak at 406.7 eV, which is the dominant characteristic feature of the N 1s spectra of lipids, is assigned to N 1s  $\rightarrow$   $\sigma^*_{C-N}$  transitions. Previous studies showed that species containing NR<sub>2</sub>H<sub>2</sub><sup>+</sup> groups do not exhibit lower energy features, whereas neutral NH<sub>2</sub> or RNH species do show a low-lying peak at 402.3 eV attributed to N 1s  $\rightarrow$   $\sigma^*_{N-H}$  transitions.<sup>45–47</sup> Thus, the low intensity but quite structured signal in the 399–404 eV range is unexpected. The weak peak around 399 eV, most prominent in DOPC, may arise from creation of N=C double bonds through radiation damage, a change noted previously.<sup>47</sup> Compared to prior NEXAFS studies, our N 1s spectra of all 3 lipids are similar in shape to the N 1s spectrum of DPPC reported by Panajotović et al.<sup>21</sup> and that of PC reported by Tsukada et al.<sup>23</sup> although our spectra are less noisy. We note a discrepancy in the energy scales, with the strong peaks appearing at 406.7 eV in our work being reported at 407.5 eV in DPPC<sup>21</sup> and at 403.5 eV in PC.<sup>23</sup> The reason for such large discrepancies is unclear.

Figure 3a presents the O 1s spectra of DOPC, DSPC, and DOTAP on OD1 intensity scales. The energies and proposed

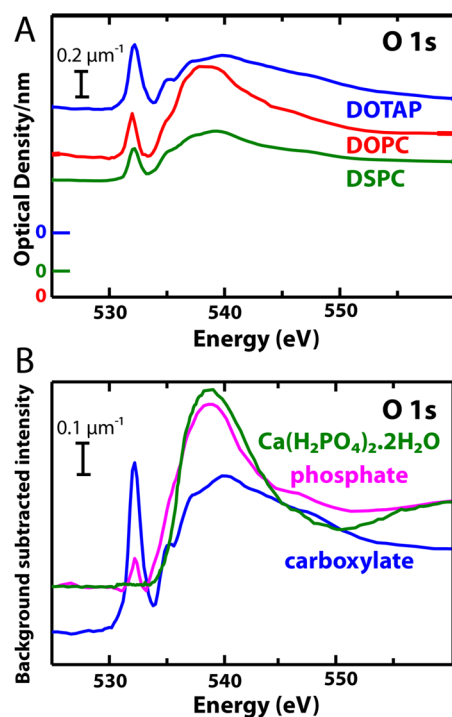


**Figure 3.** (a) O 1s spectra of DOPC, DSPC, and DOTAP, presented on an absolute OD1 intensity scale (OD/nm). (b) Background subtracted O 1s spectra of the carboxylate group (DOTAP) and phosphate group [generated from average of (DOPC – 0.5(DOTAP)) and (DSPC – 0.5(DOTAP))], with background subtraction prior to taking the difference to isolate the O1 signal. The O 1s spectrum of Ca(H<sub>2</sub>PO<sub>4</sub>)<sub>2</sub>·2H<sub>2</sub>O is also plotted for comparison.

assignments for the spectral features are listed in Table 1. While the amount of oxygen in lipids is relatively small, the characteristic O 1s  $\rightarrow$   $\pi^*$  transition at 532.1 eV from the carboxylate in the polar headgroup can be used to confirm identification of a lipid. The small peak at 535.3 eV is the O 1s(OR)  $\rightarrow$   $\pi^*(COOR)$  transition as observed in other carboxylate and carboxylic acid species. The large, broad peak at 539 eV is due to O 1s  $\rightarrow$   $\sigma^*_{O-C}$  and O 1s  $\rightarrow$   $\sigma^*_{P-O}$

transitions. The magnitude of the O 1s  $\rightarrow$   $\pi^*$  features relative to the intensity at 539 eV varies considerably among these three lipids, with the  $\pi^*$  features in DOTAP being significantly stronger than those in DOPC and DSPC. On the basis of the structure (Scheme 1), the DOPC and DSPC species have identical oxygen environments, consisting of 2 carboxylates and the phosphate group. However, DOTAP is a pure carboxylate signal since it does not have the phosphocholine. Since inner shell excitation is largely a localized excitation, it is a reasonable approximation to consider the DOPC and DSPC spectra to be a linear combination of the spectra of the carboxylate and phosphocholine groups. This additivity approximation<sup>48</sup> is likely to be particularly valid in this case, since the carboxylate and phosphocholine groups are separated by a 2-carbon aliphatic linkage which minimizes delocalization. We note that the building block concept<sup>49,50</sup> is similar; in both cases, the inner shell spectrum of a complex molecule is considered to be the sum of its parts. Manipulation of the three spectra allows us to separate the contributions of the carboxylate and the phosphate in DOPC and DSPC, thereby revealing the O 1s spectrum of the phosphate moiety of the phosphocholine group. Figure 3B plots the separated components, with that for the carboxylate being the spectrum of DOTAP and that for phosphate being the average of (DOPC – 0.5(DOTAP)) and (DSPC – 0.5(DOTAP)), in each case after a linear background subtraction to isolate only the O 1s contribution. Once the characteristic 2-peak structure of O 1s excitation in carboxylates is removed, there is very little signal at 532 eV, and the phosphate spectrum is dominated by the O 1s  $\rightarrow$   $\sigma^*_{P-O}$  transition at 539 eV, which is considerably narrower and more intense than the O 1s  $\rightarrow$   $\sigma^*_{O-C}$  transitions of the carboxylate. For comparison we also plot the O 1s spectrum of Ca(H<sub>2</sub>PO<sub>4</sub>)<sub>2</sub>·2H<sub>2</sub>O in Figure 3B. The phosphate spectrum isolated from the DOPC and DSPC O 1s spectra is in good agreement with that of Ca(H<sub>2</sub>PO<sub>4</sub>)<sub>2</sub>·2H<sub>2</sub>O, aside from the small residual 532 eV signal, from incomplete removal of the carboxylate signal.

Two groups have reported O 1s spectra of lipid materials previously. Our O 1s spectrum of DSPC is in good agreement in shape and feature energies with that of DPPC reported by Panajotović et al.<sup>21</sup> When compared to the spectrum of PC reported by Tsukada et al.,<sup>23</sup> our spectrum of DOPC is similar to that of the PC attached to Au nanoparticles, but has a shape significantly different from that of the PC sheet. In addition, the energy of the discrete O 1s  $\rightarrow$   $\pi^*$  is different: We find it at 532.1 eV, whereas Tsukada et al.<sup>23</sup> report it at 531.5 eV.

**3.2. Using STXM to Map Phase-Segregated Lipid Thin Films.** Figure 4 presents results from a C 1s spectromicroscopy study of a 12  $\mu$ m  $\times$  20  $\mu$ m area of a 50:50 molar ratio DOPC/DSPC phase-segregated film prepared by drop-casting from a 0.01 mg/mL (total lipid) chloroform solution. Figure 4a presents the C 1s spectra of the DOPC and DSPC domains extracted from the stack, in comparison to rescaled reference spectra of the pure species (cf. Figure 1). Aside from some minor shape differences in the 290–295 eV region, the spectra of the phase-segregated domains agree very well with the reference spectra. Figure 4b is the fluorescence image of the same area, which shows the distribution of DOPC (bright areas, associated with emission from DHPE-LR dye which segregates preferentially into DOPC) and DSPC (dark areas). Figure 4c is the quantitative DOPC map derived by fitting the full C 1s stack for the DOPC and DSPC reference spectra. Clearly there is very close agreement between the STXM and fluorescence

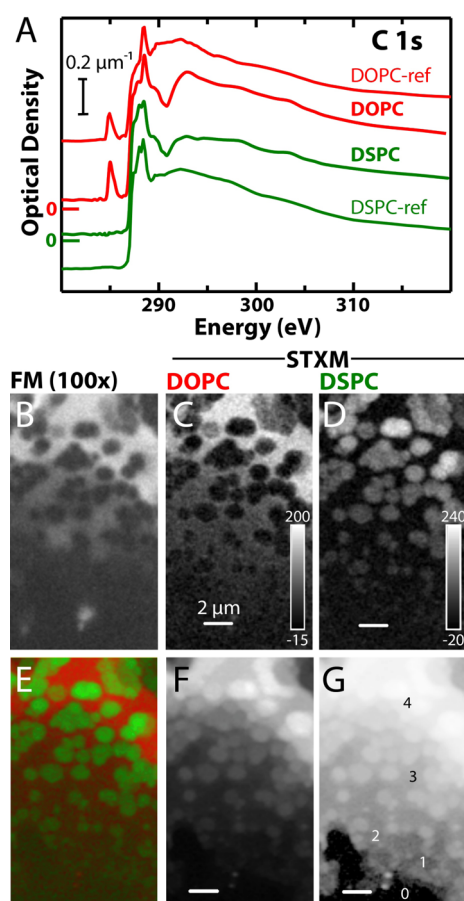


**Figure 4.** Results from FM and STXM analysis of a dry, 50:50 molar ratio DOPC/DSPC phase-segregated film deposited from chloroform. (a) C 1s spectra of DOPC-rich and DSPC-rich domains compared to reference spectra of pure DOPC and pure DSPC. (b) Fluorescence microscopy (FM) image of the  $12 \mu\text{m} \times 20 \mu\text{m}$  area studied. The signal is from a Rhodamine dye-labeled lipid (DHPE) which preferentially segregates into DOPC-rich domains. Component maps of (c) DOPC and (d) DSPC presented on absolute thickness scale. (e) Color-coded composite of the DOPC (red) and DSPC (green) component maps. (f) Sum of the DOPC and DSPC component maps. (g) log (base 10) of the total lipid thickness map which clearly indicates the presence of 4 discrete layer thicknesses (numbered). The areas labeled 1 and 2 correspond to 1 and 2 SLB layers, respectively, based on the thickness of those layers.

microscopy maps of DOPC. The only significant difference is some additional fluorescence signal in the lower center part of the fluorescence image, which may be some of the DHPE-LR dye outside of the DOPC/DSPC phase-segregated film. Figure 4d presents the quantitative DSPC map, which is mainly the complement of the DOPC map, at least in the upper region where the continuous DOPC/DSPC is located. Figure 4e is a color-coded composite of the STXM-derived component maps, based on absolute thicknesses (0–240 nm scale), with DOPC in red and DSPC in green. The thickness of the film varies in different regions and is on the order of 220 nm in the thickest part, as evident from the grayscale of the sum of the DOPC and DSPC component maps (Figure 4f). The material appears to be composed of at least 4 distinct layers, as can be better seen in the log of the total thickness map (Figure 4g). In each layer, the DOPC domain is continuous, while the discrete DSPC domains are always 10–20% (or  $\sim 1$  nm) thicker than the DOPC domain enclosing it, consistent with previous studies of

DOPC/DSPC SLBs studied through atomic force microscopy.<sup>51</sup> It has been observed previously that phase segregation occurring in stacked lipid bilayers containing DOPC/DSPC mixtures shows alignment of the domains across the bilayers in the stack,<sup>52</sup> which explains the observation of pure DOPC or DSPC regions across a region of the sample where the thickness corresponds to multiple lipid bilayers.

**3.3. Bilayer STXM.** Figure 5 presents fluorescence images of mixed DOPC/DSPC supported lipid bilayers with relative molar compositions of 75:25, 50:50, and 25:75, doped with 1

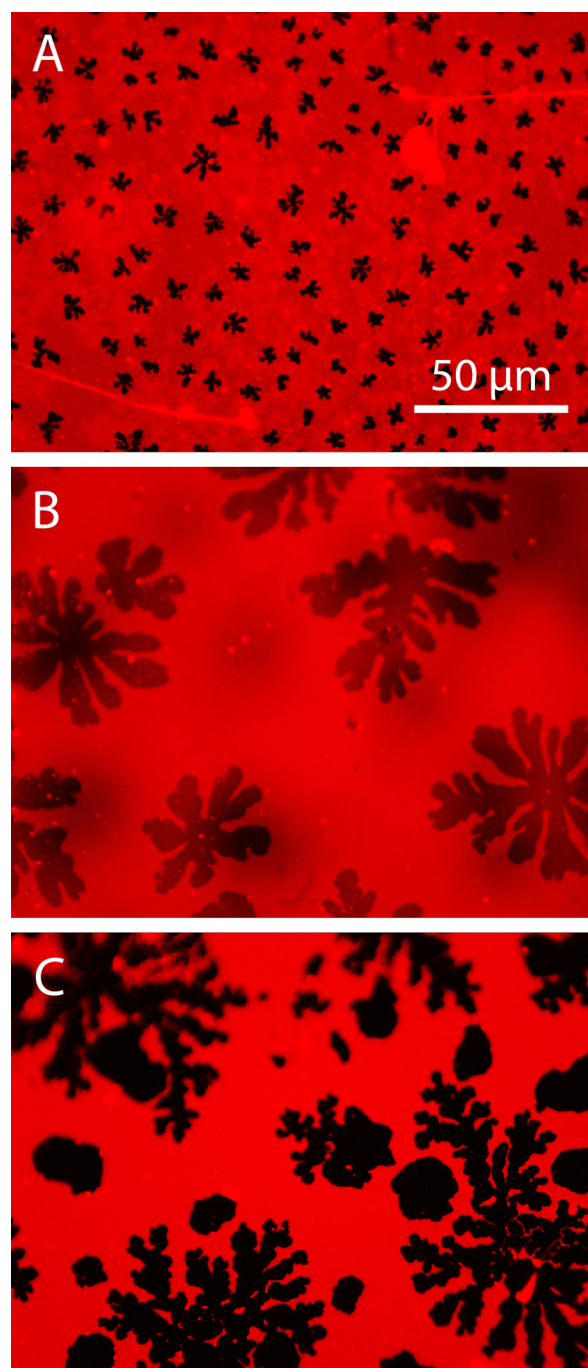


**Figure 5.** FM images of (a) 75:25, (b) 50:50, and (c) 25:75 (weight %) DOPC/DSPC phase-segregated supported lipid bilayers in 1X PBS buffer solution formed on mica using procedures described in the text.

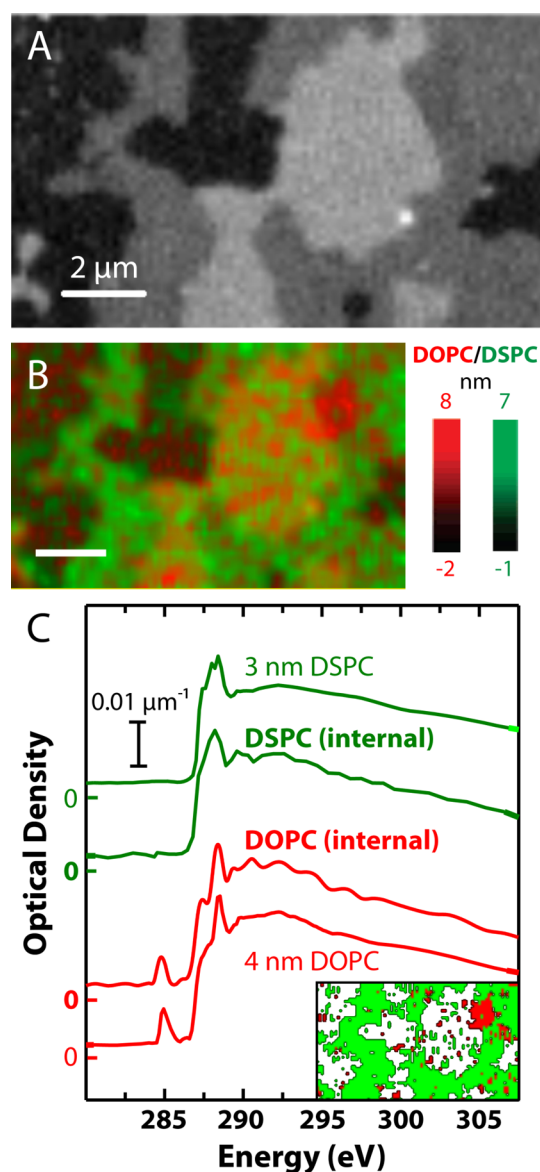
ppt of DHPE-LR for fluorescence imaging of the liquid disordered phase. The samples shown were prepared on freshly cleaved mica supports and imaged in  $1\times$  PBS buffer. When SLB preparations were done on hydrophilic treated  $\text{SiN}_x$  windows, the phase segregation process was hindered (due to stronger lipid–substrate interactions), as evidenced by the appearance of smaller DSPC domains under similar preparation conditions and incubation times. The SLB structures further degraded after the buffer solution was replaced with ultra pure deionized water and the samples were dried. While fluorescence imaging under dry conditions provided much poorer quality images than those obtained for wet samples, imaging of the dried SLB samples prior to STXM provided useful information to help locate a region of the sample that contained phase-segregated bilayer material with discrete DSPC domains.

Figure 6 presents the C 1s STXM analysis of a dried lipid sample with a DOPC/DSPC 25:75 composition which was prepared using the SUV fusion method to form SLBs in aqueous conditions. The signal intensity for the total lipid content in this image is on the order of magnitude expected for a single lipid bilayer. The overall distribution of lipids, derived from the sum of the DOPC and DSPC component maps is presented in Figure 6a. The step change in intensity and the uniform intensity within each region are highly suggestive of the presence of regions containing no bilayer (black), one bilayer (dark gray), and two bilayer (light gray) regions. Figure 6b is a color-coded composite of the DOPC (red) and DSPC (green) component maps derived by a singular value decomposition analysis of the C 1s stack. The color scales indicate the thickness of the bilayers in nanometers of each lipid component. Figure 6c compares the C 1s spectra derived from DOPC- and DSPC-rich regions to the reference spectra of pure DOPC and pure DSPC (cf. Figure 1). Clearly, the distinctive  $\pi^*_{\text{C}=\text{O}}$  carboxylate feature at 288.5 eV is present in both areas, whereas only the regions identified as being DOPC-rich exhibit the 285.1 eV signal, indicating unsaturation.

Figure 7a–d presents component maps derived from fitting a C 1s stack recorded on a 50:50 DOPC/DSPC bilayer to the C 1s OD1 reference spectra displayed in Figure 1. While the raw component maps (Figure 7a,b) have low contrast, the different lipid domains can be seen clearly after smoothing with a 5-pixel 2D Savitsky-Golay algorithm (Figure 7c,d). The thickness scales derived from the analysis are consistent with known thicknesses of single lipid bilayers.<sup>9,53</sup> Figure 7e is a color-coded composite of the smoothed DOPC (red) and DSPC (green) component maps. In order to verify the fitting results, a threshold mask was applied to the smoothed component maps to define sets of pixels that had high-DOPC or -DSPC content. Figure 8 plots the C 1s spectra extracted from the high-DOPC and high-DSPC regions, in comparison to the spectra of the pure materials. The good agreement and the clear observation of the characteristic 285 eV peak in the DOPC signal but not in the DSPC signal provide confidence in the ability of STXM to differentiate and quantitatively map spatial distributions of saturated and unsaturated lipids at the bilayer level.

#### 4. DISCUSSION

Novakova et al.<sup>12</sup> used STXM and NEXAFS spectroscopy to study lipid systems of various types, including a wet sample of a supported DPPC/DPPS (4:1) lipid bilayer in the gel phase. While they were able to detect C 1s signal from the lipid part of sample, the spectral intensity was 2–3 times larger ( $>0.02$  in the C 1s continuum) than what we measure in the true bilayer



**Figure 6.** (a) Map of all lipid content which is the sum of the DOPC and DSPC component maps derived from analysis of a C 1s image sequence ( $22\ \mu\text{m} \times 18\ \mu\text{m}$ , 45 energies from 280–310 eV). (b) Color-coded composite map of the DOPC (red) and DSPC (green) components. The as-derived component maps were subjected to a 5-point smoothed image. The color scales indicate the thickness scale of each component in nm. (c) Plot of the C 1s spectra extracted from DOPC-rich and DSPC-rich regions. The insert cartoon indicates the area of the map where the DOPC- and DSPC-rich spectra were obtained.

regime (Figure 8), and the main C 1s peak was at 287.9 eV, considerably lower than the 288.5 eV energy that we and others<sup>21–23</sup> have measured for the carboxylate group in lipids. They also used STXM to measure the C 1s spectrum of a thick deposit of 1,2-dimyristoyl-3-phosphatidylcholine (DMPC), and a separate laser plasma soft X-ray spectrometer to measure the C 1s spectra of bulk DMPS, DOPS, and DOPC. While the shapes of these reference spectra agree well with the present work, there are significant differences in the energy scales, by typically 0.5 eV. Due to the careful calibration with  $\text{CO}_2$  and  $\text{N}_2$  gas in the same time period that the spectra in Figures 1–3 were measured, we have confidence in the accuracy of the

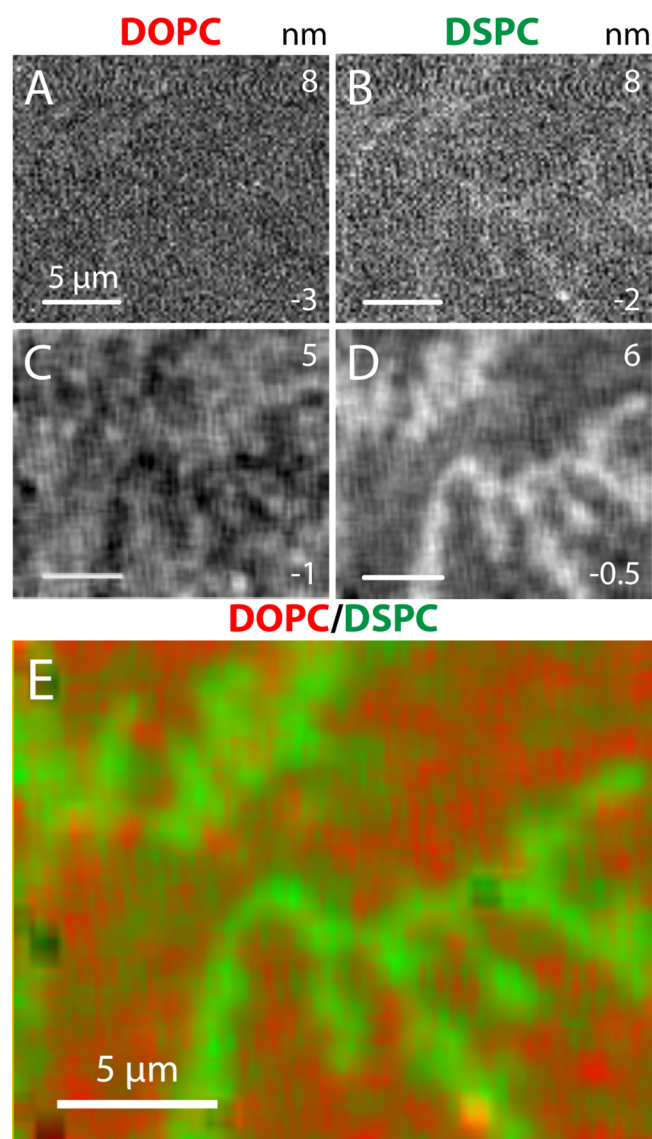


**Figure 7.** Component maps of (a) DOPC and (b) DSPC, derived by fitting a C 1s stack ( $22 \mu\text{m} \times 18 \mu\text{m}$ , 54 energies from 280–316 eV, 5 ms dwell) to the OD1 reference spectra of DOPC and DSPC shown in Figure 1. (c, d) 5-Pixel 2D Savitsky–Golay smoothed results of panels a and b. The numbers in the lower and upper right side of each map are the thickness in nm of the grayscale. (e) Color composite of the 5-pixel smoothed DOPC (red) and DSPC (green) maps.

energy scales of our spectral data. Novakova et al.<sup>12</sup> do note that the C 1s  $\rightarrow \pi^*_{\text{C}=\text{C}}$  peak at 285 eV can be used to differentiate unsaturated from saturated lipids in mixed lipid systems, but they did not demonstrate this capability as we have done in this work. Finally, as a spectroscopic study, the present work is more complete, since it reports the N 1s and O 1s spectra, and all spectra are of higher precision/accuracy over a much wider energy range. The latter is critical to accurate intensity calibration to generate OD1 reference spectra suitable for quantitative studies. Other purely spectroscopic studies<sup>21–23</sup> have been discussed in some detail in section 3.1. In general, our results are in good agreement with most of these studies; in particular, we note the commonality of a 288.3–288.5 eV feature as characteristic of all lipids and the 285.1 eV  $\pi^*_{\text{C}=\text{C}}$  peak as being present in all lipids with unsaturated chains.

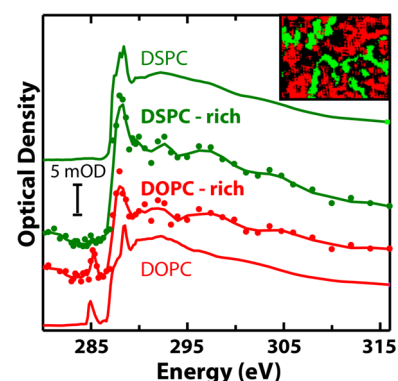


**Figure 8.** Comparison of C 1s spectra extracted from DSPC- and DOPC-rich regions using the masks indicated to define regions-of-interest (ROI). The spectra of pure DSPC and DOPC are also plotted, with an intensity given by the mean thickness of the DSPC- and DOPC-rich regions. The inset shows the DSPC- and DOPC-rich ROIs.

This study set out to define the basic spectroscopy of lipids at a more accurate level than that which had existed in the literature and to explore the ability of STXM as an analytical microscopy technique to identify and map different lipids in phase-segregated SLBs. While the basic capability of STXM to examine SLBs was explored earlier by Novakova et al.<sup>12</sup> (including measuring SLBs under  $0.5 \mu\text{m}$  water), to our knowledge this is the first demonstration of quantitative mapping of mixed lipid SLBs. This is not an easy experiment due to a number of factors. First, the signal is very weak; one must be able to measure signals at the 0.01 OD level with 5–10% precision. Second, even in the dry state, lipids are very radiation sensitive; thus, one must be cautious about the dose used. These requirements are clearly incompatible. In this work, we were able to find a compromise by using a partially defocused spot (100–200 nm) when measuring the SLBs. This work also demonstrated the importance of proper conditioning of the silicon nitride substrate. Without a suitably prepared hydrophilic surface, the samples formed very patchy SLBs which were not bilayers after drying and did not exhibit clear phase segregation.

## 5. SUMMARY

The application of STXM for identifying and quantitatively mapping lipid species in a multicomponent supported lipid bilayer is aided by accurate, calibrated, and absolute intensity reference spectra of the individual pure species. From these reference spectra (Figures 1–3), it is clear that the simplest way to differentiate saturated (e.g., DSPC) and unsaturated lipid species (e.g., DOPC and DOTAP) is by using the C 1s absorption spectrum, in particular using the C 1s(C=C)  $\rightarrow \pi^*_{\text{C}=\text{C}}$  transition at 285.1 eV to identify regions of the unsaturated component. Figures 4 and 6–8 showcase the chemical and spatial mapping capabilities of STXM. The lipids can be distinguished readily by the presence/absence of the 285.1 eV C 1s(C=C)  $\rightarrow \pi^*_{\text{C}=\text{C}}$  peak which occurs in unsaturated lipids, such as DOPC, but not in saturated lipids, such as DSPC. Although there are clear challenges associated with applying STXM to SLBs, this work has demonstrated that the experiments are feasible, if difficult. At present, our efforts are focused on developing a flow cell that will facilitate *in situ* studies of fully hydrated SLBs. Eventually, we hope to be able to use *in situ* STXM to investigate mechanisms of binding of

antimicrobial peptides to model lipid bilayers.<sup>15,16</sup> Such studies are increasingly important as bacteria become more resistant to currently available antibiotics.

## AUTHOR INFORMATION

### Corresponding Authors

\*E-mail: mirabj@mcmaster.ca.

\*E-mail: aph@mcmaster.ca.

### ORCID

Jonathan D. West: 0000-0002-4370-4425

Sokunthearath Saem: 0000-0002-9106-8160

Jose Moran-Mirabal: 0000-0002-4811-3085

Adam P. Hitchcock: 0000-0002-1598-7886

### Notes

The authors declare no competing financial interest.

## ACKNOWLEDGMENTS

This research was funded by NSERC Discovery Grants awarded to AH and JMM. AH acknowledges support of the Canada Research Chair program. JMM is the recipient of an Early Researcher Award through the Ontario Ministry of Research and Innovation and acknowledges support from CFI. YZ acknowledges partial support through the IDEM-CREATE program. STXM measurements were performed in part with the ambient STXM at the Canadian Light Source, beamline 10ID1 and in part at the polymer STXM on beamline 5.3.2.2 at the Advanced Light Source. CLS is supported by CFI, NSERC, University of Saskatchewan, WEDC, NRC and the CIHR. The Advanced Light Source is supported by the Director, Office of Energy Research, Office of Basic Energy Sciences, Materials Sciences Division of the U.S. Department of Energy, under Contract No. DE-AC02-05CH11231. We thank beamline scientists Jian Wang at CLS and David Kilcoyne at ALS, for their expert support of the instrumentation.

## REFERENCES

- (1) Mashaghi, S.; Jadidi, T.; Koenderink, G.; Mashaghi, A. Lipid Nanotechnology. *Int. J. Mol. Sci.* **2013**, *14*, 4242–4282.
- (2) Andersen, O. S.; Koeppe, R. E., II. Bilayer Thickness and Membrane Protein Function: An Energetic Perspective. *Annu. Rev. Biophys. Biomol. Struct.* **2007**, *36*, 107–130.
- (3) Sloan, C. D.; Marty, M. T.; Sligar, S. G.; Bailey, R. C. Interfacing Lipid Bilayer Nanodiscs And Silicon Photonic Sensor Arrays For Multiplexed Protein–Lipid And Protein–Membrane Protein Interaction Screening. *Anal. Chem.* **2013**, *85*, 2970–2976.
- (4) Jiang, Z.; Vasil, A. L.; Hale, J.; Hancock, R. E. W.; Vasil, M. L.; Hodges, R. S. Hodges RS. Effects Of Net Charge And The Number Of Positively Charged Residues On The Biological Activity Of Amphipathic Alpha-Helical Cationic Antimicrobial Peptides. *Adv. Exp. Med. Biol.* **2009**, *611*, 561–562.
- (5) Hancock, R.E.W. *Bacterial Structure and Physiology: Influence on Susceptibility to Cationic Antimicrobial Peptides. in Mammalian host defense peptides*; Devine, D.A., Hancock, R. E. W., Eds.; Cambridge University Press: New York, 2004; pp 229–244.
- (6) Simons, K.; Vaz, W. L. C. Model Systems, Lipid Rafts, And Cell Membranes. *Annu. Rev. Biophys. Biomol. Struct.* **2004**, *33*, 269–295.
- (7) Korlach, J.; Schwille, P.; Webb, W. W.; Feigenson, G. W. Characterization Of Lipid Bilayer Phases By Confocal Microscopy And Fluorescence Correlation Spectroscopy. *Proc. Natl. Acad. Sci. U. S. A.* **1999**, *96*, 8461–8466.
- (8) Moran-Mirabal, J. M.; Aubrecht, D. M.; Craighead, H. G. Phase Separation and Fractal Domain Formation in Phospholipid/diacetylene-Supported Lipid Bilayers. *Langmuir* **2007**, *23*, 10661–10671.

(9) Zhu, Y.; Moran-Mirabal, J. Micropatterning of Phase-Segregated Supported Lipid Bilayers and Binary Lipid Phases through Polymer Stencil Lift-Off. *Langmuir* **2016**, *32*, 11021–11028.

(10) Hitchcock, A. P. Soft X-Ray Imaging and Spectromicroscopy. In *Handbook of Nanoscopy*; Van Tendeloo, G., Van Dyck, D., Pennycook, S. J., Eds.; Wiley-VCH Verlag GmbH & Co. KGaA: Weinheim, Germany, 2012; pp 745–91.

(11) Lawrence, J. R.; Swerhone, G. D. W.; Leppard, G. G.; Araki, T.; Zhang, X.; West, M. M.; Hitchcock, A. P. Scanning Transmission X-Ray, Laser Scanning, And Transmission Electron Microscopy Mapping Of The Exopolymeric Matrix Of Microbial Biofilms. *Appl. Environ. Microbiol.* **2003**, *69*, 5543–5554.

(12) Novákova, E.; Mitrea, G.; Peth, C.; Thieme, J.; Mann, K.; Salditt, T. Solid Supported Multicomponent Lipid Membranes Studied By X-Ray Spectromicroscopy. *Biointerphases* **2008**, *3*, FB44–F54.

(13) Leung, B. O.; Brash, J. L.; Hitchcock, A. P. Characterization Of Biomaterials By Soft X-Ray Spectromicroscopy. *Materials* **2010**, *3*, 3911–3938.

(14) Leung, B. O.; Hitchcock, A. P.; Won, A.; Ianoul, A.; Scholl, A. Imaging Interactions of Cationic Antimicrobial Peptides with Model Lipid Membranes using X-ray Spectromicroscopy. *Eur. Biophys. J.* **2011**, *40*, 805–810.

(15) Won, A.; Khan, M.; Gustin, S.; Akpawu, A.; Seebun, D.; Avis, T.; Leung, B. O.; Hitchcock, A. P.; Ianoul, A. Investigating the Effects of L- to D- Amino Acid Substitution and Deamidation on the Activity and Membrane Interactions of Antimicrobial Peptide Anoplin. *Biochim. Biophys. Acta, Biomembr.* **2011**, *1808*, 1592–1600.

(16) Idiong, G.; Won, A.; Ruscito, A.; Leung, B. O.; Hitchcock, A. P.; Ianoul, A. Investigating the Effect of Single Glycine to Alanine Substitution on Membrane Interactions of Antimicrobial Peptide Latarcin 2a. *Eur. Biophys. J.* **2011**, *40*, 1087–1100.

(17) Lee, J.R.I.; Bagge-Hansen, M.; Tunuguntla, R.; Kim, K.; Bangar, M.; Willey, T. M.; Tran, I. C.; Kilcoyne, D. A.; Noy, A.; van Buuren, T. Ordering In Bio-Inorganic Hybrid Nanomaterials Probed By In Situ Scanning Transmission X-Ray Microscopy. *Nanoscale* **2015**, *7*, 9477–9486.

(18) Carrascosa, J. L.; Chichón, J. F.; Pereiro, E.; Rodríguez, M. J.; Fernández, J. J.; Esteban, M.; Heim, S.; Guttmann, P.; Schneider, G. Cryo-X-Ray Tomography Of Vaccinia Virus Membranes And Inner Compartments. *J. Struct. Biol.* **2009**, *168*, 234–239.

(19) Rightor, E. G.; Hitchcock, A. P.; Ade, H.; Leapman, R. D.; Urquhart, S. G.; Smith, A. P.; Mitchell, G.; Fischer, D.; Shin, H. J.; Warwick, T. Spectromicroscopy of Poly(ethylene Terephthalate): Comparison of Spectra and Radiation Damage Rates in X-Ray Absorption and Electron Energy Loss. *J. Phys. Chem. B* **1997**, *101*, 1950–1960.

(20) Wang, J.; Botton, G. A.; West, M. M.; Hitchcock, A. P. Quantitative Evaluation Of Radiation Damage To Polyethylene Terephthalate By Soft X-Rays And High Energy Electrons. *J. Phys. Chem. B* **2009**, *113*, 1869–1876.

(21) Panajotović, R.; Ptasinska, S.; Lyamayev, V.; Prince, K. Low-Energy Electron Damage of DPPC Molecules – A NEXAFS Study. *Radiat. Appl.* **2016**, *1*, 46–50.

(22) Franz, J.; Graham, D. J.; Schmäser, G. L.; Baio, J. E.; Lelle, M.; Peneva, K.; Müllen, K.; Castner, D. G.; Bonn, N.; Weidner, T. Full Membrane Spanning Self-Assembled Monolayers As Model Systems For UHV-Based Studies Of Cell-Penetrating Peptides. *Biointerphases* **2015**, *10*, 019009.

(23) Tsukada, C.; Tsuji, T.; Matsuo, K.; Nomoto, T.; Kutluk, G.; Sawada, M.; Ogawa, S.; Yoshida, T.; Yagi, S. Spectroscopic And Morphological Studies On Interaction Between Gold Nanoparticle And Liposome Constructed With Phosphatidylcholine. *IOP Conf. Ser.: Mater. Sci. Eng.* **2015**, *76*, 012001.

(24) West, J. D. W. *Scanning Transmission X-Ray and Fluorescence Microscopy of Lipid Bilayers*. M.Sc. thesis. McMaster University, Hamilton, ON, Canada, 2016.

(25) *Avanti Polar Lipids. Materials Safety Data Sheets.* [https://avantilipids.com/images/MSDS/AvantiPolarLipids\\_SDS\\_840458P.pdf](https://avantilipids.com/images/MSDS/AvantiPolarLipids_SDS_840458P.pdf) (accessed on November 15, 2016).

- (26) Ratto, T. V.; Longo, M. L. Obstructed Diffusion in Phase-Separated Supported Lipid Bilayers: A Combined Atomic Force Microscopy and Fluorescence Recovery after Photobleaching Approach. *Biophys. J.* **2002**, *83*, 3380–3392.
- (27) Kraft, M. L.; Weber, P. K.; Longo, M. L.; Hutcheon, I. D.; Boxer, S. G. Phase Separation of Lipid Membranes Analyzed with High-Resolution Secondary Ion Mass Spectrometry. *Science* **2006**, *313*, 1948–1951.
- (28) Mantil, E.; Crippin, T.; Ianoul, A.; Avis, T. J. Experimental Parameters Leading to Optimal Bilayers for Total Internal Reflection Fluorescence Microscopy Visualization. *Microsc. Microanal.* **2017**, *23*, 97–112.
- (29) Seu, K. J.; Pandey, A. P.; Haque, F.; Proctor, E. A.; Ribbe, A. E.; Hovis, J. S. Effect of Surface Treatment on Diffusion and Domain Formation in Supported Lipid Bilayers. *Biophys. J.* **2007**, *92*, 2445–2450.
- (30) Ricker, J. V.; Tsvetkova, N. M.; Wolkers, W. F.; Leidy, C.; Tablin, F.; Longo, M.; Crowe, J. H. Trehalose Maintains Phase Separation in an Air-Dried Binary Lipid Mixture. *Biophys. J.* **2003**, *84*, 3045–3051.
- (31) Kilcoyne, A. L. D.; Tyliczszak, T.; Steele, W. F.; Fakra, S.; Hitchcock, P.; Franck, K.; Anderson, E.; Harteneck, B.; Rightor, E. G.; Mitchell, G. E.; Hitchcock, A. P.; et al. Interferometrically Controlled Scanning Transmission Microscopes at the Advanced Light Source. *J. Synchrotron Radiat.* **2003**, *10*, 125–136.
- (32) Warwick, T.; Ade, H.; Kilcoyne, A. L. D.; Kritscher, M.; Tyliczszak, T.; Fakra, S.; Hitchcock, A. P.; Hitchcock, P.; Padmore, H. A. A New Bend Magnet Beam Line for Scanning Transmission X-ray Microscopy at the Advanced Light Source. *J. Synchrotron Radiat.* **2002**, *9*, 254–257.
- (33) Kaznatcheev, K. V.; Karunakaran, Ch.; Lanke, U. D.; Urquhart, S. G.; Obst, M.; Hitchcock, A. P. Soft X-ray Spectromicroscopy Beamline at the CLS: Commissioning Results. *Nucl. Instrum. Methods Phys. Res., Sect. A* **2007**, *582*, 96–99.
- (34) Jacobsen, C.; Wirick, S.; Flynn, G.; Zimba, C. Soft X-ray Spectroscopy from Image Sequences with Sub-100 nm Spatial Resolution. *J. Microsc.* **2000**, *197*, 173–184.
- (35) Hitchcock, A. P. *aXis2000*, 2016. Written in IDL and available free for non-commercial use from <http://unicorn.mcmaster.ca/aXis2000.html>.
- (36) Koprinarov, I. N.; Hitchcock, A. P.; McCrory, C.; Childs, R. F. Quantitative Mapping of Structured Polymeric Systems Using Singular Value Decomposition Analysis of soft X-ray Images. *J. Phys. Chem. B* **2002**, *106*, 5358–5364.
- (37) Henke, B. L.; Gullikson, E. M.; Davis, J. C. X-Ray Interactions: Photoabsorption, Scattering, Transmission, And Reflection At  $E = 50\text{--}30000$  eV,  $Z = 1\text{--}92$ . *At. Data Nucl. Data Tables* **1993**, *54*, 181–342.
- (38) Rankin, D. W. H. In *CRC Handbook Of Chemistry And Physics*; Lide, D. R., Ed.; CRC Press: Boca Raton, FL, 2009; pp 223–224.
- (39) Koenig, B. W.; Gawrisch, K. Specific Volumes Of Unsaturated Phosphatidylcholines In The Liquid Crystalline Lamellar Phase. *Biochim. Biophys. Acta, Biomembr.* **2005**, *1715*, 65–70.
- (40) Urquhart, S. G.; Ade, H. Trends in the Carbonyl Core (C 1s, O 1s)  $\rightarrow \pi^*$  C=O Transition in the Near-Edge X-ray Absorption Fine Structure Spectra of Organic Molecules. *J. Phys. Chem. B* **2002**, *106*, 8531–8538.
- (41) Benzerara, K.; Yoon, T. H.; Tyliczszak, T.; Constantz, B.; Spormann, A. M.; Brown, G. E. Scanning Transmission X-Ray Microscopy Study Of Microbial Calcification. *Geobiology* **2004**, *2*, 249–259.
- (42) Cody, G. D.; Ade, H.; Wirick, S.; Mitchell, G. D.; Davis, A. Determination Of Chemical-Structural Changes In Vitrinite Accompanying Luminescence Alteration Using C-NEXAFS Analysis. *Org. Geochem.* **1998**, *28*, 441–455.
- (43) Lehmann, J.; Liang, B.; Solomon, D.; Lerotic, M.; Luizão, F.; Kinyangi, J.; Schäfer, T.; Wirick, S.; Jacobsen, C. Near-edge X-ray Absorption Fine Structure (NEXAFS) Spectroscopy For Mapping Nano-Scale Distributions Of Organic Forms In Soil: Application To Black Carbon Particles. *Global Biogeochem. Cycles* **2005**, *19*, GB1013.
- (44) Schumacher, M.; Christl, I.; Scheinost, A. C.; Jacobsen, C.; Kretzschmar, R. Chemical Heterogeneity Of Organic Soil Colloids Investigated By Scanning Transmission X-Ray Microscopy and C-1s NEXAFS Microspectroscopy. *Environ. Sci. Technol.* **2005**, *39*, 9094–9099.
- (45) Gordon, M. L.; Cooper, G.; Morin, C.; Araki, T.; Turci, C. C.; Kaznatcheev, K.; Hitchcock, A. P. Inner-Shell Excitation Spectroscopy Of The Peptide Bond: Comparison of the C 1s, N 1s, and O 1s Spectra Of Glycine, Glycyl-Glycine, And Glycyl-Glycyl-Glycine. *J. Phys. Chem. A* **2003**, *107*, 6144–6159.
- (46) Otero, E.; Urquhart, S. G. Nitrogen 1s Near-Edge X-ray Absorption Fine Structure Spectroscopy of Amino Acids: Resolving Zwitterionic Effects. *J. Phys. Chem. A* **2006**, *110*, 12121–12121.
- (47) Messer, B. M.; Cappa, C. D.; Smith, J. D.; Wilson, K. R.; Gilles, M. K.; Cohen, R. C.; Saykally, R. J. pH Dependence of the Electronic Structure of Glycine. *J. Phys. Chem. B* **2005**, *109*, 5375–5382.
- (48) Cooper, G.; Gordon, M.; Tulumello, D.; Turci, C. C.; Kaznatcheev, K.; Hitchcock, A. P. Inner Shell Excitation Of Glycine, Glycyl-Glycine, Alanine And Phenylalanine. *J. Electron Spectrosc. Relat. Phenom.* **2004**, *137–140*, 795–799.
- (49) Stöhr, J. *NEXAFS Spectroscopy*; Springer Tracts in Surface Science 25; Springer: Berlin, 1992.
- (50) Stewart-Ornstein, J.; Hitchcock, A. P.; Hernández-Cruz, D.; Henklein, P.; Overhage, J.; Hilpert, K.; Hale, J.; Hancock, R. E. W. Using Intrinsic X-Ray Absorption Spectral Differences to Identify and Map Peptides and Proteins. *J. Phys. Chem. B* **2007**, *111*, 7691–7699.
- (51) Spurlin, T. A.; Gewirth, A. A. Charge Dependence of a Nanoscale Supercrystal Phase in a Supported Lipid Bilayer. *J. Am. Chem. Soc.* **2007**, *129*, 11906–11907.
- (52) Zhu, Y.; Negmi, A.; Moran-Mirabal, J. M. Multi-Stacked Supported Lipid Bilayer Micro Patterning Through Polymer Stencil Lift-Off. *Membranes* **2015**, *5*, 385–398.
- (53) El Kirat, K.; Morandat, S.; Dufrene, Y. F. Nanoscale Analysis of Supported Lipid Bilayers Using Atomic Force Microscopy. *Biochim. Biophys. Acta, Biomembr.* **2010**, *1798*, 750–765.
- (54) Ma, Y.; Chen, C. T.; Meigs, G.; Randall, K.; Sette, F. High-Resolution K-Shell Photoabsorption Measurements of Simple Molecules. *Phys. Rev. A: At, Mol., Opt. Phys.* **1991**, *44*, 1848–1852.
- (55) Chen, C. T.; Ma, Y.; Sette, F. K-shell Photoabsorption of the N<sub>2</sub> Molecule. *Phys. Rev. A: At, Mol., Opt. Phys.* **1989**, *40*, 6737–6742.
- (56) Hitchcock, A. P.; Ishii, I. Carbon K-Shell Excitation Spectra of Linear and Branched Alkanes. *J. Electron Spectrosc. Relat. Phenom.* **1987**, *42*, 11–26.